Extreme Mechanics Letters 21 (2018) 49–56

Contents lists available at ScienceDirect

Extreme Mechanics Letters

journal homepage: www.elsevier.com/locate/eml

Dielectric-elastomer-based capacitive force sensing with tunable and enhanced sensitivity

Jian Cheng [a], Zheng Jia [b,c,*], Teng Li [a,*]

[a] Department of Mechanical Engineering, University of Maryland, College Park, MD 20742, United States
[b] Department of Engineering Mechanics, Zhejiang University, Hangzhou 310027, China
[c] Key Laboratory of Soft Machines and Smart Devices of Zhejiang Province, Zhejiang University, Hangzhou 310027, China

ARTICLE INFO

Article history:
Received 21 February 2018
Received in revised form 23 March 2018
Accepted 26 March 2018
Available online 8 April 2018

Keywords:
Soft force sensor
Enhanced sensitivity
Tunable sensitivity
Dielectric elastomer

ABSTRACT

Designing capacitive force sensors with an enhanced and *in situ* tunable sensitivity is important in many fields such as robotic grippers but has been challenging. Existing capacitive force sensors mainly rely on ingenious but complex structural designs, posing tremendous difficulty in fabrication and usually featuring a fixed sensitivity. We present a facile design of capacitive tactile force sensor with an enhanced and tunable sensitivity using electro-mechanically responsive dielectric elastomer as the sensing medium. Dielectric elastomer exhibits tunable mechanical properties when subject to voltage and pre-stretch: increasing voltage and pre-stretch level leads to a more compliant response to the external pressure. Effectively, the sensitivity of the dielectric elastomer sensor can be continuously increased over one order of magnitude by properly exerting voltage and pre-stretch to the dielectric elastomer tactile sensor.

1. Introduction

To perform touching, gripping, pushing, and pulling, human hands count on the tactile feedback from nerve endings, which are densely populated on palm skin [1,2]. These nerve endings, working collaboratively to form a sensory network, feature a capability of detecting tactile forces across a range of several orders of magnitude with correspondingly appropriate sensitivities [3,4]. Recent research has suggested that human hands are sufficiently sensitive to perceive the haptic interaction with a nanoscale-featured surface [5], whereas in other extreme scenarios it also sustains force of a few hundred pounds when lifting a barbell set. As an artificial analog of human skin, smart skin is a micro-electro-mechanical system (MEMS) that can sense the force of different magnitudes and accurately track the force variation. Although the large-range or multi-resolution feature may be fulfilled through ingenious structural designs [6–9] on the systems level, the complication in MEMS fabrication imposes tremendous difficulty in employing such an approach, posing a significant challenge to the tactile sensor development. An alternative approach that circumvents the complex fabrication processes would be leveraging smart materials that exhibit tunable mechanical behaviors. In this letter, we present a design of dielectric elastomer (DE) normal force sensor with enhanced and tunable sensitivity, facilitated by modulating the mechanical property of DE *in situ* by electro-mechanical stimuli.

DE is a soft matter that can deform dramatically in response to both mechanical and electrical stimuli. DE is classified as an electroactive polymer as it operates by converting changes of voltage to mechanical deformation. When subject to voltage, a piece of DE sandwiched between two thin conductive coating layers (as shown schematically in Fig. 1a) contracts in the direction of the applied voltage and expands its normal area. Because of its electroactive behavior and large deformability, DE has been studied extensively as soft actuators with a myriad of applications in artificial muscles [10–13], soft transducers [14–16], and soft robotics [2,17–23]. On the other hand, a sandwich architecture of dielectric elastomer actuator (DEA) in Fig. 1a naturally forms a deformable capacitor, of which the capacitance is directly tuned by the deformation of DE. This fact has inspired researchers to integrate the capacitance measurement functionality into the drive circuit of DEA to bestow deformation feedback to the actuator itself, enabling simultaneous mechanical actuation and strain sensing [2,24–30]. Thus more advanced controllability can be achieved through accurate real-time displacement inquiry [29,30]. Significant progresses aside, how to enhance and tune the sensitivity of DE sensors remains much less studied.

A remarkable but often neglected aspect of DE is that the effective mechanical property also changes upon the application of electrical field [31–33]. That is, the application of voltage induces opposite charges on the top and bottom surfaces of the DE piece,

* Corresponding authors.
E-mail addresses: zheng.jia@zju.edu.cn (Z. Jia), lit@umd.edu (T. Li).

https://doi.org/10.1016/j.eml.2018.03.004
2352-4316/

furthermore generates a resultant electrostatic pressure, and effectively squeezes the piece in the normal direction. This electrostatic pressure serves as an auxiliary force and works synergistically with the mechanical load acting on the structure. In the existence of such an electrostatic auxiliary pressure, to deform the DE piece to the same extent, a lower mechanical load is needed than in the absence of the applied voltage, or a larger strain can be achieved with the same level of mechanical load. Equivalently, the DE piece becomes more compliant; moreover, the extra deformability depends on the voltage difference placed on the top and bottom electrodes. Therefore, by changing the voltage difference, the mechanical response of DE can be altered in a controllable manner. The modulation of the effective stiffness of the sensing medium is essential for manipulating the sensor sensitivity. Utilizing the *in situ* adjustable mechanical property of DE, therefore, represents a promising route towards advanced tactile force sensing with a tunable and enhanced sensitivity. Such an approach, to our best knowledge, has not been reported previously in the development of soft capacitive sensors or other soft tactile sensors, for example soft resistive sensors [34–37].

2. Deformation of a DE force sensor under pressure and voltage

A piece of DE layer deforms when subject to a distributed force F and a voltage V, and the dimensions in the original state L_1, L_2, and L_3 become l_1, l_2, and l_3, respectively. The deformation behavior of DE essentially resembles a hyperelastic material whose mechanical response can be derived from a free energy density function, except for that DE is responsive to both mechanical and electrical loads. It is stipulated that the free energy is composed of electrical and mechanical terms. In the deformed state, a generic form of the DE free energy density function is $w(\Lambda_1, \Lambda_1, \Lambda_3, D)$ with $\Lambda_1 = l_1/L_1$, $\Lambda_2 = l_2/L_2$, $\Lambda_3 = l_3/L_3$ denoting the stretch ratios and D representing the electric displacement. In accordance with the continuum mechanics convention, the free energy density of a deformed DE can be defined in the reference state as $W\left(\Lambda_1, \Lambda_2, \Lambda_3, \tilde{D}\right)$, where $\tilde{D}$ is the corresponding nominal electric displacement. As aforementioned, the energy stored in DE stems from two origins: the mechanical work done by the pressure on the deformation and the electrical work done by the power supply through the charge redistribution. Therefore, the variation of free energy density is

$$\delta W\left(\Lambda_1, \Lambda_2, \Lambda_3, \tilde{D}\right) = S_1\delta\Lambda_1 + S_2\delta\Lambda_2 + S_3\delta\Lambda_3 + \tilde{E}\delta\tilde{D} \tag{1}$$

where $S_i = \partial W/\partial\Lambda_i$ ($i = 1, 2$, and 3) is the nominal stress, and $\tilde{E} = \partial W/\partial\tilde{D}$ is the nominal electric field, which is defined in the undeformed state. Note that the nominal electric field can be related to the applied voltage V through $V = \tilde{E}L_1$. When the DE piece is connected to a constant voltage supply through a closed circuit, V and $\tilde{E}$ both remain constant. The free energy of a DE is then

$$W\left(\Lambda_1, \Lambda_2, \Lambda_3, \tilde{D}\right) = W_s\left(\Lambda_1, \Lambda_2, \Lambda_3\right) + W_E\left(\Lambda_1, \Lambda_2, \Lambda_3, \tilde{D}\right) \tag{2}$$

where the first term W_s denotes the energy due to stretching the polymeric network in the absence of applied voltage, and the following term W_E is the energy due to dielectric polarization.

In attempt to construct a specific form of the free energy function W, we suppose that the polymeric network follows the constitutive model by Gent [38], which captures the network stiffening effect at elevated strain levels,

$$W_s = -\frac{\mu J_m}{2}\log\left(1 - \frac{I_1 - 3}{J_m}\right) \tag{3}$$

where μ is the initial shear modulus, $I_1 = \Lambda_1^2 + \Lambda_2^2 + \Lambda_3^2$ is the first invariant of right Cauchy–Green deformation tensor, and $J_m = I_m - 3$, I_m is the limiting value of I_1. The strain energy is infinitely large when I_1 reaches its limiting value I_m, thus J_m is a quantity representing the maximum possible deformation. Note that μ and J_m are two material properties that can be determined experimentally [39,40].

For the free energy arising from the dielectric polarization, to account for quasilinear and nonpolar dielectric behavior, we follow the quadratic approximation proposed by Zhao and Suo [41,42]:

$$W_E = \Lambda_1\Lambda_2^{-1}\Lambda_3^{-1}\varepsilon^{-1}\tilde{D}^2/2 \tag{4}$$

where $\varepsilon = \varepsilon_r\varepsilon_0$, ε_r is the relative permittivity of DE, and $\varepsilon_0 = 8.854\times10^{-12}$ F/m is the permittivity of vacuum. The voltage is applied in the direction of L_1, as illustrated in Fig. 1b.

When a dielectric elastomer deforms, the change in shape is usually much more pronounced than that in volume [17,19,41–43]. Consequently, it is reasonable to include the incompressibility constraint on the three stretches, i.e., $\Lambda_1\Lambda_2\Lambda_3 = 1$. To implement this constraint, we add a term $\Pi(\Lambda_1\Lambda_2\Lambda_3 - 1)$ to the free energy function W, where Π is a Lagrange multiplier. Therefore, considering Eqs. (1)–(4) and the incompressibility condition, the nominal stresses can be calculated respectively,

$$S_1 = \left.\frac{\partial W}{\partial\Lambda_1}\right|_{\Lambda_2,\Lambda_3,\tilde{D}} = \frac{\partial W_s}{\partial\Lambda_1} + \frac{1}{2\varepsilon}\Lambda_2^{-1}\Lambda_3^{-1}\tilde{D}^2 + \Pi\Lambda_2\Lambda_3 \tag{5a}$$

$$S_2 = \left.\frac{\partial W}{\partial\Lambda_2}\right|_{\Lambda_1,\Lambda_3,\tilde{D}} = \frac{\partial W_s}{\partial\Lambda_2} - \frac{1}{2\varepsilon}\Lambda_1\Lambda_2^{-2}\Lambda_3^{-1}\tilde{D}^2 + \Pi\Lambda_1\Lambda_3 \tag{5b}$$

$$S_3 = \left.\frac{\partial W}{\partial\Lambda_3}\right|_{\Lambda_1,\Lambda_2,\tilde{D}} = \frac{\partial W_s}{\partial\Lambda_3} - \frac{1}{2\varepsilon}\Lambda_1\Lambda_2^{-1}\Lambda_3^{-2}\tilde{D}^2 + \Pi\Lambda_1\Lambda_2 \tag{5c}$$

as well as the nominal electric field,

$$\tilde{E} = \left.\frac{\partial W}{\partial\tilde{D}}\right|_{\Lambda_1,\Lambda_2,\Lambda_3} = \frac{1}{\varepsilon}\Lambda_1\Lambda_2^{-1}\Lambda_3^{-1}\tilde{D} \tag{6}$$

Eqs. (5) and (6) are the equations of the state of DE. Note that the nominal electric field $\tilde{E}$ is directly related to the voltage V through $\tilde{E} = V/L_1$. Substituting Eq. (6) into Eq. (5) gives

$$S_1 = \frac{\partial W_s}{\partial\Lambda_1} + \frac{1}{2}\Lambda_1^{-2}\Lambda_2\Lambda_3\varepsilon\tilde{E}^2 + \Pi\Lambda_2\Lambda_3 \tag{7a}$$

$$S_2 = \frac{\partial W_s}{\partial\Lambda_2} - \frac{1}{2}\Lambda_1^{-1}\Lambda_3\varepsilon\tilde{E}^2 + \Pi\Lambda_1\Lambda_3 \tag{7b}$$

$$S_3 = \frac{\partial W_s}{\partial\Lambda_3} - \frac{1}{2}\Lambda_1^{-1}\Lambda_2\varepsilon\tilde{E}^2 + \Pi\Lambda_1\Lambda_2 \tag{7c}$$

When the DE sensor is compressed uniaxially in its thickness direction, it expands equal-biaxially in the two in-plane directions, resulting in $\Lambda_2 = \Lambda_3$. Substituting the incompressibility condition $\Lambda_2 = \Lambda_3 = \Lambda_1^{-1/2}$ into Eq. (7) we have

$$\frac{S_1}{\mu} - \frac{S_{2,3}}{\mu}\Lambda^{-\frac{3}{2}} = \frac{\Lambda - \Lambda^{-2}}{1 - J_m^{-1}\left(\Lambda^2 + 2\Lambda^{-1} - 3\right)} + \frac{1}{\Lambda^3}\left(\frac{\tilde{E}}{\sqrt{\mu/\varepsilon}}\right)^2 \tag{8}$$

where $\Lambda = \Lambda_1$ characterizes the deformation of the sensor. Since the deformation is homogeneous throughout the DE sensor unit, the nominal pressure applied to the DE sensor equals the corresponding nominal stress component, namely $-P_1 = S_1$. Eq. (8) relates the inputs of a DE sensor, i.e., the normal pressure P_1 and applied nominal electric field intensity $\tilde{E}$, to the output, i.e., its deformation Λ. Therefore, Eq. (8) governs the electro-mechanical response of the DE sensor.

3. Sensitivity of the DE capacitive force sensor

The configuration of DE sandwiched between conforming thin film electrodes (Fig. 1) spontaneously forms a deformable capacitor, of which the capacitance can be related to the deformation

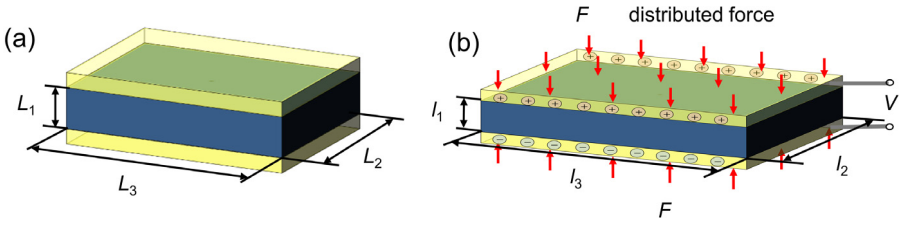

Fig. 1. (a) Schematic of a dielectric elastomer (DE) sensor unit cell in its pristine state, dimensions of the DE (the blue part) are given by L_1, L_2, and L_3; and (b) when deformed in response to the applied voltage V and distributed force F, the dimensions become l_1, l_2, and l_3. The yellow parts represent elastomeric conductive electrodes coated on the two sides of DE. (For interpretation of the references to color in this figure legend, the reader is referred to the web version of this article.)

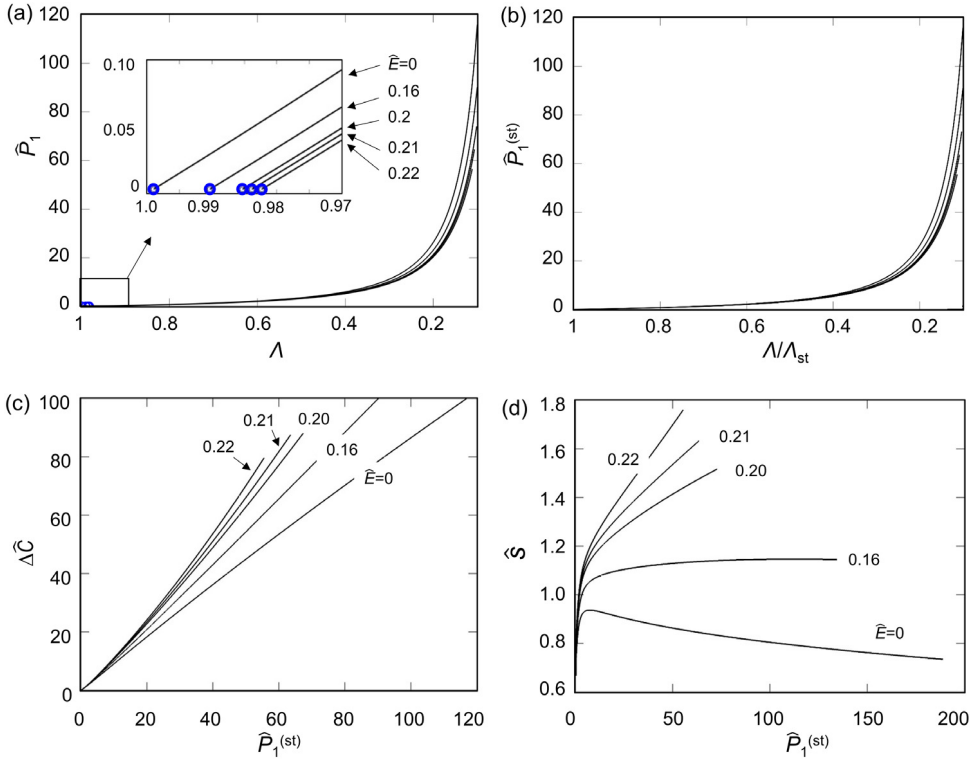

Fig. 2. Electro-mechanical response of the DE force sensor in absence of in-plane pre-stretch. The normalized applied pressure is plotted as a function of the stretch ratio with respect to (a) the original state and (b) the starting state. The normalized voltages $\hat{E} = 0$, 0.16, 0.20, 0.21, and 0.22. Blue circles mark the initial compression due to voltage application. Variation of (c) output capacitance signal and (d) sensitivity with applied normal stress. (For interpretation of the references to color in this figure legend, the reader is referred to the web version of this article.)

through

$$C = \frac{\varepsilon a}{l_1} = \frac{\varepsilon A}{\Lambda^2 L_1} \tag{9}$$

where $a = l_2 l_3$ denotes the deformed surface area, and $A = L_2 L_3$ is the area in the reference state. When the DE sensor is compressed, the thickness reduces and the area expands, leading to a decreased Λ and an increased capacitance C.

The total force exerting on the DE sensor can be calculated as

$$F = P_1 A \tag{10}$$

The sensitivity of a sensor is defined as the change in output signal per unit change in input. Therefore, taking derivative of C with respect to P_1 yields

$$s = \frac{dC}{dP_1} = \frac{dC}{d\Lambda} \cdot \frac{d\Lambda}{dP_1} \tag{11}$$

For simplicity, we further define some dimensionless groups: $\widehat{S}_i = S_i/\mu$, $\widehat{P}_i = P_i/\mu$, $\hat{E} = \tilde{E}/\sqrt{\mu/\varepsilon}$, $\hat{V} = V/(L_1\sqrt{\mu/\varepsilon})$, $\hat{C} = C/(\varepsilon A/L_1)$, and $\hat{s} = s/(\varepsilon A/\mu L_1)$. In this work, we use the representative values of material properties of 3M™ VHB series, a commercially available acrylic DE: the initial shear modulus $\mu = 250$ kPa, relative permittivity $\varepsilon_r = 6.0, J_m = 125$ [41–45], the typical dimensions for a capacitive sensor unit are $L_1 = 20$ μm, $L_2 = L_3 = 1$ mm. With these parameters, the highest voltage applied to the sensor will be ∼300 V during the working of a DE force sensor, which is modest compared to the kV level voltage applied to DE actuators [46].

4. DE force sensor without pre-stretch

In absence of the voltage, the sandwiched dielectric architecture reduces to a regular elastomer force sensor. For an as-fabricated sensor unit, neither the material property nor the resultant input–output dependence is to be altered. By contrast, the mechanical behavior of DE can be varied by changing the applied voltage. Eq. (8) suggests a family of stress–deformation relations parameterized by different values of $\tilde{E}$, namely $\Lambda\left(S_1, S_{2,3} \middle| \tilde{E}\right)$. When there exists no lateral load, $S_{2,3} = 0$ and $S_1 = -P_1$. Eq. (8)

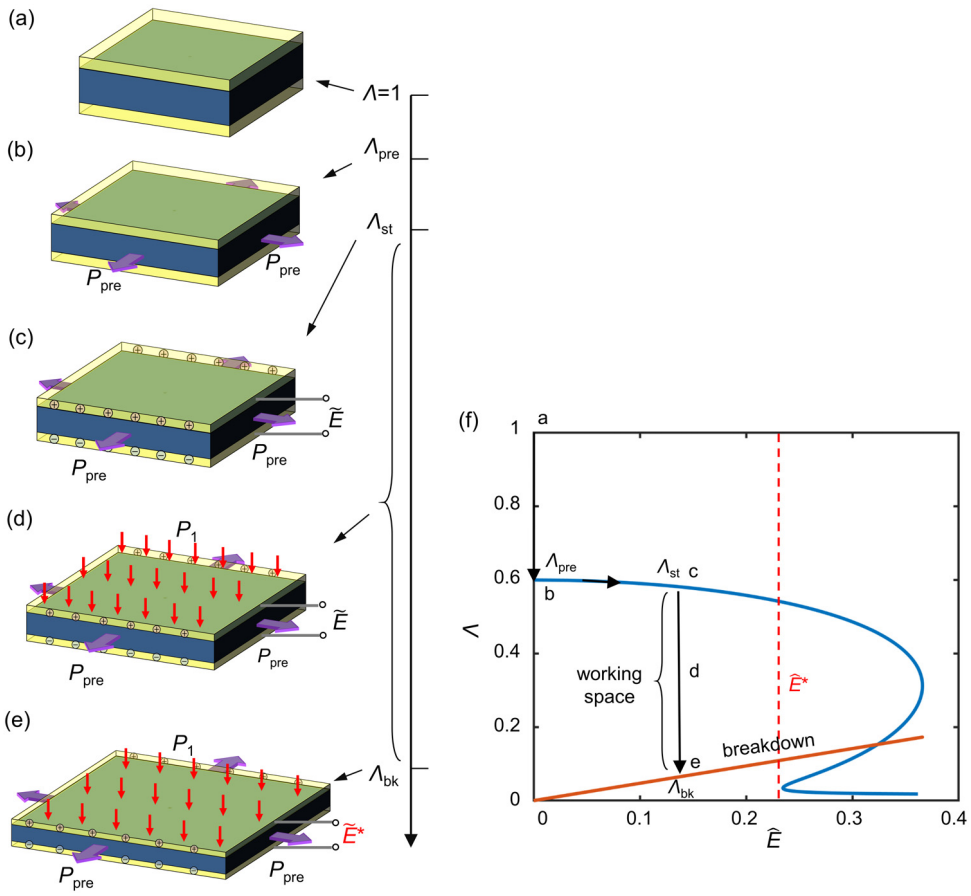

Fig. 3. Left: Schematic of the states of a DE force sensor in sequence. From (a) the pristine state, bi-lateral stresses bring the sensor to (b) the pre-strain state Λ_{pre}. The sensor attains its (c) starting state Λ_{st}, after a voltage of $\hat{E}$ is imposed to the electrodes. Then it deforms further to (d) the working state upon the application of normal pressure. Within the working state, the sensor converts the pressure change into the change of capacitance. The DE sensor fails once it reaches (e) the dielectric breakdown state. Right: (f) Sensing procedure from *a* to *e* represented in the $\Lambda \sim \hat{E}$ diagram, with the actuation curve (in blue) and the breakdown line (in orange). The critical voltage $\hat{E}^*$ is illustrated by the red dashed line. (For interpretation of the references to color in this figure legend, the reader is referred to the web version of this article.)

can then be reduced to

$$\widehat{P_1} = \frac{P_1}{\mu} = -\frac{\Lambda - \Lambda^{-2}}{1 - J_m^{-1}\left(\Lambda^2 + 2\Lambda^{-1} - 3\right)} - \frac{1}{\Lambda^3}\left(\frac{\tilde{E}}{\sqrt{\mu/\varepsilon}}\right)^2 \tag{12}$$

Fig. 2 plots the dimensionless pressure $\hat{P}_1$ as a function of the deformation Λ at various $\hat{E}$ levels. Note that Λ denotes the length ratio in the compression direction, therefore a smaller value of Λ reflects a larger deformation. For the same deformation, those DE sensors subject to a higher voltage experience a lower stress. The stress reduction can be interpreted as follows: in the procedure of compressing the sensor, the power supply is constantly providing energy by pumping charges onto the DE/electrode interfaces, the energy increase associated with dielectric polarization is $W_E = \frac{1}{2}\Lambda^{-2}\varepsilon\tilde{E}^2$; with the electric work serving as an auxiliary, to carry the sensor unit to the same deformation, the required work done by the applied stress is therefore lowered. For $\Lambda = 0.12$ (denoting a deformation where the DE is compressed to 12% of its original thickness) and $\hat{E} = 0$, the dimensionless nominal pressure $\hat{P}_1 = 77.84$, whereas the dimensionless pressure reduces to 49.84 if $\hat{E} = 0.22$. By switching on the voltage, the effective mechanical stiffness of the DE layer shows a decline of 36%.

It is worth noting that, before the pressure is applied to the sensor, the voltage itself has deformed the DE sensor to a starting state, which is labeled by the blue circles in Fig. 2 inset. During this process the electric potential energy is the sole driving force of the deformation, hence the DE sensor is actually working in the actuation mode. The deformation associated with this starting state is characterized by Λ_{st} which is determined by Eq. (8) with the vanishing stress condition, namely $\Lambda_{\text{st}} = \Lambda\left(S_1 = 0, S_{2,3} = 0 \middle| \tilde{E}\right)$. Subsequently, from these starting states the device starts to act as a sensor. Since the stresses are to be applied on top of these existing deformations, it is more convenient to recognize the starting states of DE sensors as the reference states to quantify the force loading exerted to the sensor. Then the nominal pressure defined in the new reference configuration is given by $\hat{P}_1^{(\text{st})} = \hat{P}_1(\Lambda_{2,3}^{(\text{st})})^{-2} = \hat{P}_1\Lambda_{\text{st}}$, and the corresponding deformation can be calculated as $\Lambda/\Lambda_{\text{st}}$. Fig. 2b plots the $\hat{P}_1^{(\text{st})} \sim \Lambda/\Lambda_{\text{st}}$ relation.

Upon deformation the measurable output, namely the normalized capacitance change is

$$\Delta\hat{C} = \frac{\Delta C}{\varepsilon A/L_1} = \frac{1}{\Lambda^2} - \frac{1}{\Lambda_{\text{st}}^2} \tag{13}$$

where ΔC denotes the increase in capacitance upon the normal pressure application from the sensor's starting deformation. The normalized capacitance change $\Delta\hat{C}$ is plotted as a function of the applied pressure $\hat{P}_1^{(\text{st})}$ in Fig. 2c. At a given voltage, the capacitance increases monotonically with increasing $\hat{P}_1^{(\text{st})}$ suggesting that the capacitance change can be used to measure the applied pressure. For a fixed $\hat{P}_1^{(\text{st})}$ a higher voltage yields a larger capacitance change, as a result of the effective softening of the DE. For example, when $\hat{P}_1^{(\text{st})} = 50$, $\Delta\hat{C} = 44.92$ in the absence of voltage and $\Delta\hat{C} = 70.01$ with $\hat{E} = 0.22$. The derivative of $\Delta\hat{C}$ with respect to $\hat{P}_1^{(\text{st})}$ yields the dimensionless sensitivity $\hat{s}$. It is worth noting that due to the

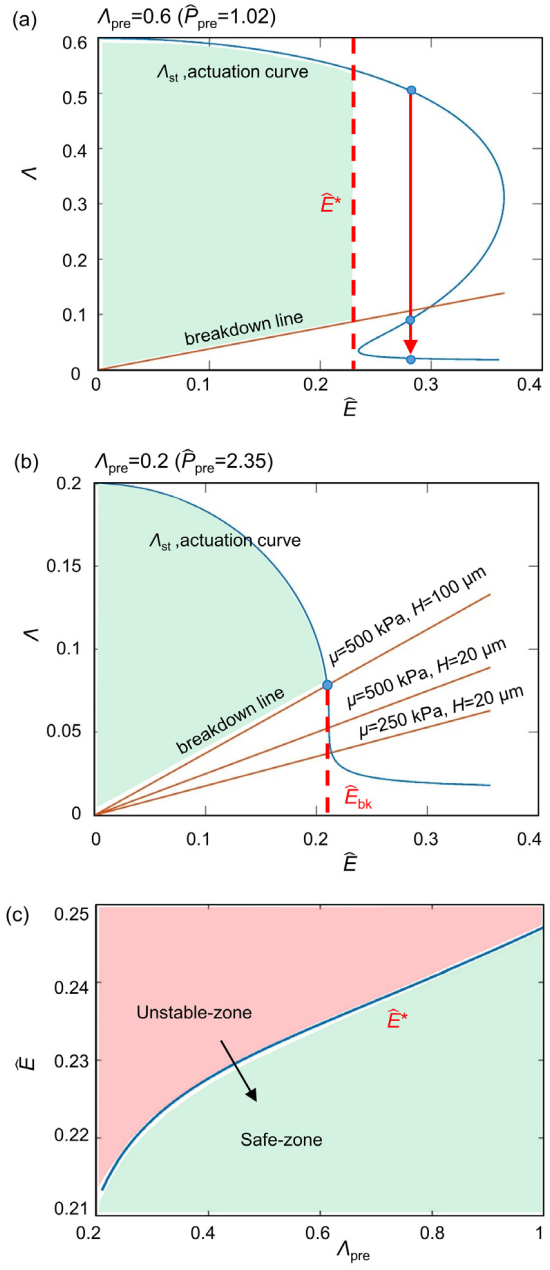

Fig. 4. Working range (a) At $\hat{P}_{pre} = 1.02$, and the corresponding pre-stretch deformation $\Lambda_{pre} = 0.6$, the actuated starting states form an S-shaped curve on $\Lambda \sim \hat{E}$ diagram. Beyond the critical voltage $\hat{E}^*$, snap-through instability occurs and the DE sensor collapses from $\Lambda = 0.54$ to 0.06 (shown by the red arrow), penetrating the breakdown line, and leading to electrical breakdown. (b) When $\hat{P}_{pre} = 2.35$, the pre-stretch state is $\Lambda_{pre} = 0.2$, and the actuation curve of the starting states is single-valued. The breakdown voltage is identified by the point where the actuation curve and breakdown line intersect. The breakdown line varies with material properties and geometric parameters of the DE sensor. (c) Instability critical voltage $\hat{E}^*$ for given pre-stretch. The $\hat{E}^* \sim \Lambda_{pre}$ separates the unstable-zone from the safe-zone. The arrows represent two ways of avoiding instability. (For interpretation of the references to color in this figure legend, the reader is referred to the web version of this article.)

form of Eq. (12), an explicit expression of $\hat{s}$ as a function of $\hat{P}_1^{(st)}$ is not available analytically, but can be obtained numerically by combining Eqs. (11)–(13). As shown in Fig. 2d, a DE force sensor with a higher applied voltage possesses enhanced sensitivity; for example, the peak sensitivity varies approximately from 0.73 to 1.76 for $\hat{E}$ in the range of 0∼0.22. Moreover, with a modest applied voltage (e.g. from $\hat{E} = 0.16$ to $\hat{E} = 0.22$), the sensitivity of the DE sensor keeps increasing as the applied pressure increases, indicating that the DE sensor is more sensitive in detecting pressure change at a high pressure range.

In this section, we investigate the effect of voltage on the sensitivity enhancement. It is demonstrated that a higher voltage leads to an increased sensitivity. However, an elevated voltage beyond a proper scope may lead to electro-mechanical failure of the sensor, which will be systematically discussed in next section.

5. DE force sensor with pre-stretch

It has been demonstrated that the sensitivity of a DE sensor can be enhanced by applying a voltage; however, the increase of sensor sensitivity due to the application of the voltage is still not pronounced, exemplified by the fact that the peak sensitivity only changes by a factor of 2.41 when the voltage ramps from $\hat{E} = 0$ to $\hat{E} = 0.22$. To overcome this deficiency, we further propose a strategy to remarkably enhance the sensitivity by pre-stretching the DE sensor prior to the voltage application.

In addition, upon electrical actuation, the DE layer is susceptible to a snap-through phase separation known as electro-mechanical instability [2,18,23,42,47,48]. Pre-stretching the DE piece is also proved to be an effective approach to achieving large deformation of dielectric elastomer actuator (DEA) and attenuating the electro-mechanical instability [18].

Specifically, before the application of voltage, a pre-stretched state of the DE sensor can be achieved by equal-biaxially stretching the DE piece in the in-plane directions through applying a pair of pre-stresses of fixed value P_{pre}, as depicted in Fig. 3b. Such a fixed pre-stress can be implemented by using a dead load. Due to the incompressibility, the DE layer shrinks in the thickness direction, and the compression ratio can be calculated as $\Lambda_{pre} = \Lambda_1^{(pre)} = \left[\Lambda_{2,3}^{(pre)}\right]^{-2}$. Λ_{pre} represents the compression in the thickness direction after the application of the pre-stress P_{pre}. In this paper, we use Λ_{pre} to identify the pre-stretched state of the sensor. The lateral stress needed to achieve this pre-stretch can be determined by Eq. (8) with $\hat{S}_1 = 0$ and $\hat{E} = 0$,

$$\hat{P}_{pre} = -\frac{\Lambda_{pre}^{\frac{5}{2}} - \Lambda_{pre}^{-\frac{1}{2}}}{1 - J_m^{-1}\left(\Lambda_{pre}^2 + 2\Lambda_{pre}^{-1} - 3\right)} \tag{14}$$

For example, if $\Lambda_{pre} = 0.6$, i.e., the thickness becomes 60% of its original value during pre-stretch, the required lateral stress is $\hat{P}_{pre} = 1.02$. The arrow pointing from *a* to *b* indicates this pre-stretch process in Fig. 3f.

On top of the pre-stretched deformation, a modest voltage $\hat{E}$ is applied. The DE layer is further deformed by the electric actuation to a starting state *c*, as shown in Fig. 3. The starting state deformation Λ_{st} is the solution to Eq. (8), with the lateral stresses determined by Eq. (14), i.e., $\Lambda_{st} = \Lambda\left(\hat{S}_1 = 0, \hat{P}_{pre} \middle| \hat{E}\right)$. The deformation due to voltage actuation follows the *bc* segment of the blue actuation curve in Fig. 3f. Once arrives at the starting state, the DE piece is ready to function as a sensor. Upon the application of the pressure P_1, the DE sensor works within the *pressure sensing* mode and deforms from *c* towards *d* as shown in Fig. 3f. In this regime, the output capacitance change is measured to reflect the applied force.

As the thickness of the sensor decreases with the applied pressure, the electrical field intensity continuously rises. The DE sensor may work safely until the DE layer deforms to a certain thickness $l_{bk} = L_1\Lambda_{bk}$ such that the true electric field reaches the dielectric breakdown threshold E_{bk}. The limit deformation is hence specified by Λ_{bk}. Therefore the range from Λ_{st} to Λ_{bk} is the working range

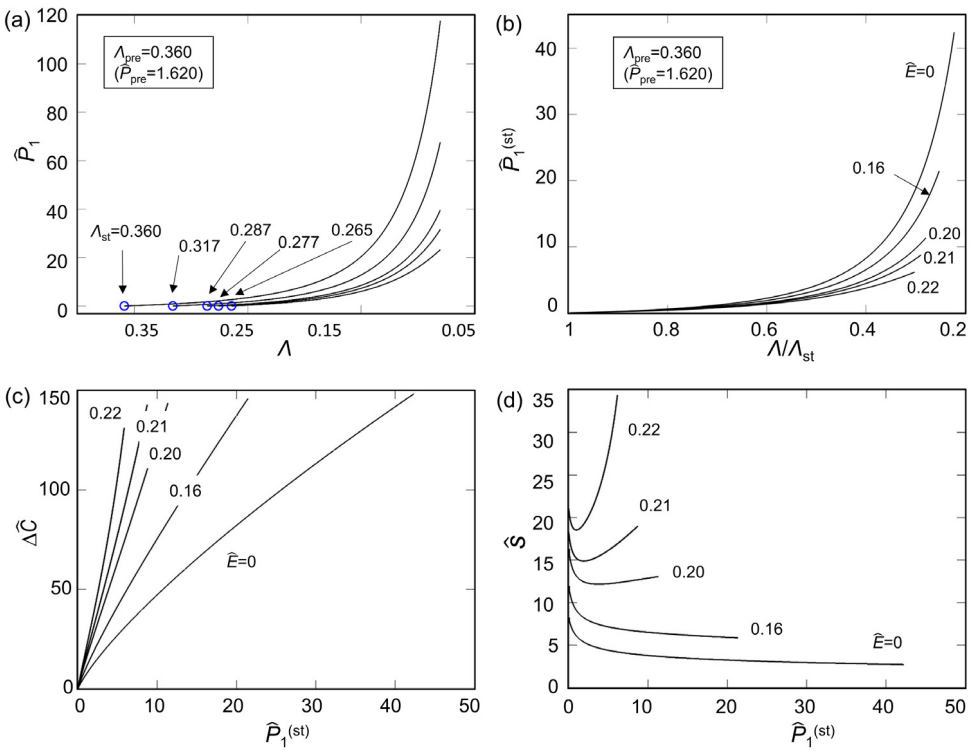

Fig. 5. Force–deformation relation at $\hat{P}_{pre} = 1.62$, ($\Lambda_{pre} = 0.36$) with different applied voltages $\hat{E} = 0$, 0.16, 0.20, 0.21, and 0.22, using (a) the original state and (b) the starting state as the reference state. Blue circles mark the starting states. (c) Dimensionless capacitance output signal and (d) sensitivity at $\Lambda_{pre} = 0.36$. (For interpretation of the references to color in this figure legend, the reader is referred to the web version of this article.)

of the DE sensor, which is represented by the line segment *cde* in Fig. 3f. The corresponding pressure range is $0 \sim P_{bk}$, where P_{bk} is the maximum applied pressure which brings the DE sensor to the breakdown state. Rather than remaining as a fixed value, it is reported that the breakdown electric field intensity E_{bk} depends on the thickness as well as the pre-stretch level [2,43,49]. According to Huang et al. [43], E_{bk} (in V/m) of acrylic DE follows the empiric power law,

$$E_{bk} = 161.3 L_1^{-0.25} \Lambda_{pre}^{-0.565} \tag{15}$$

where L_1 denotes the pristine thickness (in μm), and Λ_{pre} is the compression ratio of the thickness due to pre-stretch. Consequently, the breakdown deformation can be expressed as $\Lambda_{bk} = \frac{\sqrt{\mu/\varepsilon}}{E_{bk}}\hat{E}$, which forms the straight orange line in the $\Lambda \sim E$ diagram in Fig. 3f.

To avoid electrical breakdown, it is crucial to identify the maximum voltage that can be exerted to the DE sensor. During actuation process (state *b* to *c*), once the applied voltage $\hat{E}$ increases beyond a threshold value $\hat{E}^*$ (indicated by the red dashed line in Fig. 3f), for a given $\hat{E}$ there exist more than one associated equilibrium states. As shown in Fig. 4a, at the critical voltage $\hat{E}^* = 0.235$ the two possible equilibrium deformations are $\Lambda = 0.54$ and $\Lambda = 0.06$, respectively, which marks a nine-time difference in thickness. When subject to a perturbation, the DE sensor may shift between these co-existing equilibrium states with an abrupt change in the deformation Λ. Such an abrupt change in thickness caused by snap-through instability is generally hazardous for DE, since the collapsed state may fall underneath the breakdown line, as illustrated by the red arrow in Fig. 4a. In these cases, electrical breakdown fails the DE sensor even prior to the application of any force. In order to avoid such failure, the applied voltage $\hat{E}$ should remain below the critical voltage $\hat{E}^*$.

The electro-mechanical instability is mitigated by tuning the pre-stretch level of the DE sensor. Comparing Fig. 4a with b, one may conclude that the actuation curve evolves from an S-shaped curve at a modest pre-stretch ($\hat{P}_{pre} = 1.02$, $\Lambda_{pre} = 0.6$) to a monotonously decreasing curve at an elevated pre-stretch ($\hat{P}_{pre} = 2.35$, $\Lambda_{pre} = 0.2$), consequently the electro-mechanical instability disappears. Although critical voltage $\hat{E}^*$ for electro-mechanical instability does not exist for sensors with $\Lambda_{pre} \leq 0.20$, the intersection of breakdown line and actuation curve identifies a breakdown voltage $\hat{E}_{bk}$, i.e. the highest voltage that can be exerted on the DE sensor with $\Lambda_{pre} \leq 0.20$. Beyond $\hat{E}_{bk}$, the sensor failures by electrical breakdown before it could reach the starting state.

Given a combination of Λ_{pre} and $\hat{E}$, upon a normal pressure, the continuous deformation of the DE sensor tracks a vertical line connecting the starting state on and the electrical breakdown limit. All the admissible working states of a DE sensor is highlighted by the green region in Fig. 4a and b. For pre-stretch $\Lambda_{pre} = 0.6$, the actuation curve, breakdown curve, and voltage threshold $\hat{E}^*$ demarcate a trapezoid-like region representing the working states. In comparison, if $\Lambda_{pre} = 0.20$, the working states of the sensor constitute a fan-liked region, as shown in Fig. 4b. Moreover, since the breakdown line is determined by the original thickness and the material properties, i.e., $\Lambda_{bk} = \frac{\sqrt{\mu/\varepsilon}}{E_{bk}}\hat{E}$, the electrical breakdown line can be tilted by reducing the original thickness or selecting DE material with smaller $\sqrt{\mu/\epsilon}$. Changing these parameters may expand the working zone of the DE sensor as shown in Fig. 4b. Fig. 4c shows the critical voltage $\hat{E}^*$ as a function of pre-stretch Λ_{pre}. The green-shaded area beneath the $\hat{E}^* \sim \Lambda_{pre}$ curve is the safe zone, whereas the red-shaded area is the failure zone where electrical breakdown occurs due to snap-through instability. The arrows in Fig. 4c indicate two ways of avoiding the abrupt collapse: using a lower voltage or reducing the pre-stretch level.

We next study the load–deformation relation of DE sensor within the working zone. With a pre-stress of $\hat{P}_{pre} = 1.62$, (the pre-stretch deformation $\Lambda_{pre} = 0.36$), the $\hat{P}_1 \sim \Lambda$ characteristic curves are drawn in Fig. 5a with a series of normalized voltage $\hat{E}$. The

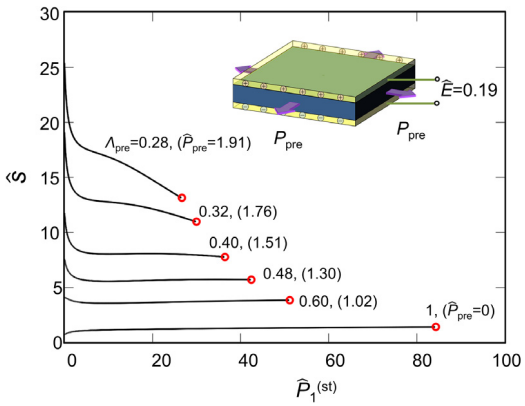

Fig. 6. Dimensionless sensitivity at various pre-stretch levels with a fixed voltage $\hat{E} = 0.19$. The red circles at the end of each curve represent the final states, i.e., at which the sensor fails by electrical breakdown. (For interpretation of the references to color in this figure legend, the reader is referred to the web version of this article.)

blue circles mark the starting states of each sensor. The required normal stress to deform the DE sensor to a certain extent is further reduced compared with cases without pre-stretch as shown in Fig. 2a; the DE material is made more compliant by pre-stretching the sensor prior to the voltage application. Fig. 5b plots the pressure/deformation relation with respect to the starting states for each sensor.

The output capacitive signal $\Delta\hat{C}$ is plotted against $\hat{P}_1^{(st)}$ in Fig. 5c and the sensitivity $\hat{s}$ is shown in Fig. 5d. $\hat{s}$ varies from 2.73 to 34.4, which is approximately twenty times as the largest sensitivity in absence of pre-stretch. Fig. 6 shows how the sensitivity scales up with the pre-stretch level. At same applied voltage $\hat{E} = 0.19$, $\hat{s}$ increases by one order of magnitude when pre-strain deformation changes from 1 to 0.28. The sensitivity of the DE normal force sensor fabricated with the identical material can be tuned over a large range ($\hat{s} = 0.73$ when no pre-strain or voltage applied; $\hat{s} = 34.4$ at $\hat{E} = 0.22$ and $\hat{P}_{pre} = 1.62$) through the combination of pre-stretch and applying voltage. As we point out, pre-stretching and applying voltage provides a facile approach to achieving tunable and enhanced sensing capability of DE force sensor. Such an approach of utilizing sensing media with modifiable mechanical properties to fulfill tunable sensitivity is also applicable to the development of other soft sensors.

6. Conclusion

The present design using DE as the sensing medium has demonstrated the possibility to achieve *in situ* tunable and enhanced sensitivity, which is in sharp contrast to the traditional force sensor designs with a fixed sensitivity. The tunable sensitivity is attributed to the fact that the effective mechanical property of DE sensor can be modulated through pre-stretch and voltage. To characterize the design of the DE force sensor, we identified four stages of such a DE sensor: the pre-stretch state upon the bi-lateral pre-stretch, the starting state upon application of voltage, the working state under normal stress, and the final state at the dielectric breakdown limit. We further investigated the failure mode of the DE sensor by studying the electromechanical instability at the actuation stages and its effect on the working range of the DE sensor. By simply leveraging the combination of pre-stretch and voltage, the *in situ* sensitivity can be enhanced by a factor of 47.12. Moreover, the tunable and enhanced sensitivity is achieved by only changing the voltage and pre-stretch. Such a facile design strategy may find applications in robot skins and shed light on using advanced materials in novel tactile sensor designs.

Acknowledgment

TL and JC are grateful for the support of NASA (Grant number: NNX12AM02G).

References

[1] M.H. Dickinson, C.T. Farley, R.J. Full, M.A.R. Koehl, R. Kram, S. Lehman, M.H. Dickinson, C.T. Farley, R.J. Full, M.A.R. Koehl, R. Kram, S. Lehman, Animals move: An integrative view, 288 (2013) 100–106. http://dx.doi.org/10.1126/science.288.5463.100.

[2] I.A. Anderson, T.A. Gisby, T.G. McKay, B.M. O'Brien, E.P. Calius, Multi-functional dielectric elastomer artificial muscles for soft and smart machines, J. Appl. Phys. 112 (2012). http://dx.doi.org/10.1063/1.4740023.

[3] K.G. Pearson, J.E. Misiaszek, K. Fouad, Enhancement and resetting of locomotor activity by muscle afferents, Ann. New York Acad. Sci. (1998) 203–215. http://dx.doi.org/10.1111/j.1749-6632.1998.tb09050.x.

[4] J. Duysens, F. Clarac, H. Cruse, Load-regulating mechanisms in gait and posture: comparative aspects, Physiol. Rev. 80 (2000) 83–133. http://dx.doi.org/10.1152/physrev.2000.80.1.83.

[5] L. Skedung, M. Arvidsson, J.Y. Chung, C.M. Stafford, B. Berglund, M.W. Rutland, Feeling small: Exploring the tactile perception limits, Sci. Rep. 3 (2013) 2617. http://dx.doi.org/10.1038/srep02617.

[6] R. Okazaki, M. Sato, S. Fukushima, M. Furukawa, H. Kajimoto, Tactile enhancement structure mimicking hair follicle receptors, in: 2011 IEEE World Haptics Conf., IEEE, 2011, pp. 335–337. http://dx.doi.org/10.1109/WHC.2011.5945508.

[7] S. Tsuji, A tactile and proximity sensor by optical and electrical measurement, in: 2012 IEEE Sensors, IEEE, 2012, pp. 1–4. http://dx.doi.org/10.1109/ICSENS.2012.6411050.

[8] S. Yao, Y. Zhu, Wearable multifunctional sensors using printed stretchable conductors made of silver nanowires, Nanoscale 6 (2014) 2345–2352. http://dx.doi.org/10.1039/c3nr05496a.

[9] Youngseok Kim, Namsun Chou, Sohee Kim, Highly sensitive capacitive tactile sensor based on silver nanowire using parylene-C stencil patterning method, in: 2015 IEEE Sensors, IEEE, 2015, pp. 1–3. http://dx.doi.org/10.1109/ICSENS.2015.7370251.

[10] T. Lu, J. Huang, C. Jordi, G. Kovacs, R. Huang, D.R. Clarke, Z. Suo, Dielectric elastomer actuators under equal-biaxial forces, uniaxial forces, and uniaxial constraint of stiff fibers, Soft Matter. 8 (2012) 6167. http://dx.doi.org/10.1039/c2sm25692d.

[11] K. Lee, S. Tawfick, Fiber micro-architected electro–elasto-kinematic muscles, Extrem. Mech. Lett. 8 (2016) 64–69. http://dx.doi.org/10.1016/J.EML.2016.03.003.

[12] Y. Wang, J. Zhu, Artificial muscles for jaw movements, Extrem. Mech. Lett. 6 (2016) 88–95. http://dx.doi.org/10.1016/J.EML.2015.12.007.

[13] T. Lu, Z. Shi, Q. Shi, T.J. Wang, Bioinspired bicipital muscle with fiber-constrained dielectric elastomer actuator, Extrem. Mech. Lett. 6 (2016) 75–81. http://dx.doi.org/10.1016/J.EML.2015.12.008.

[14] R. Kaltseis, C. Keplinger, R. Baumgartner, M. Kaltenbrunner, T. Li, P. Mächler, R. Schwödiauer, Z. Suo, S. Bauer, Method for measuring energy generation and efficiency of dielectric elastomer generators, Appl. Phys. Lett. 99 (2011) 162904. http://dx.doi.org/10.1063/1.3653239.

[15] E. Bortot, M. Gei, Harvesting energy with load-driven dielectric elastomer annular membranes deforming out-of-plane, Extrem. Mech. Lett. 5 (2015) 62–73. http://dx.doi.org/10.1016/J.EML.2015.09.009.

[16] D. Peter, R. Pichler, S. Bauer, R. Schwödiauer, Electrostatic converter with an electret-like elastomer membrane for large scale energy harvesting of low density energy sources, Extrem. Mech. Lett. 4 (2015) 38–44. http://dx.doi.org/10.1016/J.EML.2015.07.008.

[17] R.E. Pelrine, R.D. Kornbluh, J.P. Joseph, Electrostriction of polymer dielectrics with compliant electrodes as a means of actuation, Sensors Actuators A Phys. 64 (1998) 77–85. http://dx.doi.org/10.1016/S0924-4247(97)01657-9.

[18] R. Pelrine, R. Kornbluh, Q. Pei, J. Joseph, High-speed electrically actuated elastomers with strain greater than 100%, Science 287 (2000) 836–839. http://dx.doi.org/10.1126/science.287.5454.836.

[19] M. Duduta, R.J. Wood, D.R. Clarke, Multilayer dielectric elastomers for fast, programmable actuation without prestretch, Adv. Mater. (2016). http://dx.doi.org/10.1002/adma.201601842.

[20] C. Keplinger, J.-Y. Sun, C.C. Foo, P. Rothemund, G.M. Whitesides, Z. Suo, Stretchable, transparent, ionic conductors, Science 341 (2013) 984–987. http://dx.doi.org/10.1126/science.1240228.

[21] S. Kim, C. Laschi, B. Trimmer, Soft robotics: A bioinspired evolution in robotics, Trends Biotechnol. 31 (2013) 287–294. http://dx.doi.org/10.1016/j.tibtech.2013.03.002.

[22] K. Jung, J.C. Koo, J. Nam, Y.K. Lee, H.R. Choi, Artificial annelid robot driven by soft actuators, Bioinspir. Biomim. 2 (2007) S42–S49. http://dx.doi.org/10.1088/1748-3182/2/2/S05.

[23] M.T. Petralia, R.J. Wood, Fabrication and analysis of dielectric-elastomer minimum-energy structures for highly-deformable soft robotic systems, in:

IEEE/RSJ 2010 Int. Conf. Intell. Robot. Syst. IROS 2010 - Conf. Proc. 0, 2010, pp. 2357–2363. http://dx.doi.org/10.1109/IROS.2010.5652506.
[24] C. Keplinger, M. Kaltenbrunner, N. Arnold, S. Bauer, Capacitive extensometry for transient strain analysis of dielectric elastomer actuators, Appl. Phys. Lett. 92 (2008) 192903. http://dx.doi.org/10.1063/1.2929383.
[25] O.A. Araromi, A. Poulin, S. Rosset, M. Imboden, M. Favre, M. Giazzon, C. Martin-Olmos, F. Sorba, M. Liley, H. Shea, Optimization of thin-film highly-compliant elastomer sensors for contractility measurement of muscle cells, Extrem. Mech. Lett. 9 (2016) 1–10. http://dx.doi.org/10.1016/J.EML.2016.03.017.
[26] T.A. Gibsy, S. Xie, E.P. Calius, I.A. Anderson, Integrated sensing and actuation of muscle-like actuators, in: Proc. SPIE 7287, Electroact. Polym. Actuators Devices 2009, 2009: p. 728707. http://dx.doi.org/10.1117/12.815645.
[27] Q. Pei, M. Rosenthal, S. Stanford, H. Prahlad, R. Pelrine, Multiple-degrees-of-freedom roll actuators, Smart Mater. Struct. 13 (2004) N86–N92. http://dx.doi.org/10.1016/B978-0-08-047488-5.00009-5.
[28] S. Son, N.C. Goulbourne, Dynamic response of tubular dielectric elastomer transducers, Int. J. Solids Struct. 47 (2010) 2672–2679. http://dx.doi.org/10.1016/j.ijsolstr.2010.05.019.
[29] T.A. Gisby, B.M. O'Brien, S.Q. Xie, E.P. Calius, I.A. Anderson, Closed loop control of dielectric elastomer actuators, in: Proc. SPIE 7976, Electroact. Polym. Actuators Devices, 2011: pp. 797620–797628. http://dx.doi.org/10.1117/12.880711.
[30] K. Jung, K.J. Kim, H.R. Choi, A self-sensing dielectric elastomer actuator, Sensors Actuators, A Phys. 143 (2008) 343–351. http://dx.doi.org/10.1016/j.sna.2007.10.076.
[31] E.G. Barnwell, W.J. Parnell, I.D. Abrahams, Tunable elastodynamic band gaps, Extrem. Mech. Lett. 12 (2017) 23–29. http://dx.doi.org/10.1016/J.EML.2016.10.009.
[32] Y.S. Teh, S.J.A. Koh, Giant continuously-tunable actuation of a dielectric elastomer ring actuator, Extrem. Mech. Lett. 9 (2016) 195–203. http://dx.doi.org/10.1016/J.EML.2016.07.002.
[33] U. Gupta, H. Godaba, Z. Zhao, C.K. Chui, J. Zhu, Tunable force/displacement of a vibration shaker driven by a dielectric elastomer actuator, Extrem. Mech. Lett. 2 (2015) 72–77. http://dx.doi.org/10.1016/J.EML.2015.02.004.
[34] H.H. Chou, A. Nguyen, A. Chortos, J.W.F. To, C. Lu, J. Mei, T. Kurosawa, W.G. Bae, J.B.H. Tok, Z. Bao, A chameleon-inspired stretchable electronic skin with interactive colour changing controlled by tactile sensing, Nature Commun. 6 (2015) 1–10. http://dx.doi.org/10.1038/ncomms9011.
[35] L. Viry, A. Levi, M. Totaro, A. Mondini, V. Mattoli, B. Mazzolai, L. Beccai, Flexible three-axial force sensor for soft and highly sensitive artificial touch, Adv. Mater. 26 (2014) 2659–2664. http://dx.doi.org/10.1002/adma.201305064.
[36] D.M. Vogt, Y.-L. Park, R.J. Wood, Design and characterization of a soft multi-axis force sensor using embedded microfluidic channels, IEEE Sens. J. 13 (2013) 4056–4064. http://dx.doi.org/10.1109/JSEN.2013.2272320.
[37] M. Shikida, T. Shimizu, K. Sato, K. Itoigawa, Active tactile sensor for detecting contact force and hardness of an object, Sensors Actuators A Phys. 103 (2003) 213–218. http://dx.doi.org/10.1016/S0924-4247(02)00336-9.
[38] A.N. Gent, A new constitutive relation for rubber, Rubber Chem. Technol. 69 (1996) 59–61. http://dx.doi.org/10.5254/1.3538357.
[39] J. Huang, T. Li, C.C. Foo, J. Zhu, D.R. Clarke, Z. Suo, Giant, voltage-actuated deformation of a dielectric elastomer under dead load, Appl. Phys. Lett. 100 (2012) 41911. http://dx.doi.org/10.1063/1.3680591.
[40] R. Kaltseis, C. Keplinger, S.J. Adrian Koh, R. Baumgartner, Y.F. Goh, W.H. Ng, A. Kogler, A. Tröls, C.C. Foo, Z. Suo, S. Bauer, Natural rubber for sustainable high-power electrical energy generation, RSC Adv. 4 (2014) 27905–27913. http://dx.doi.org/10.1039/C4RA03090G.
[41] Z. Suo, Theory of dielectric elastomers, Acta Mech. Solida Sin. 23 (2010) 549–578. http://dx.doi.org/10.1016/S0894-9166(11)60004-9.
[42] X. Zhao, Z. Suo, Electrostriction in elastic dielectrics undergoing large deformation, J. Appl. Phys. 104 (2008) 123530. http://dx.doi.org/10.1063/1.3031483.
[43] J. Huang, S. Shian, R.M. Diebold, Z. Suo, D.R. Clarke, The thickness and stretch dependence of the electrical breakdown strength of an acrylic dielectric elastomer, Appl. Phys. Lett. 101 (2012). http://dx.doi.org/10.1063/1.4754549.
[44] T.G. McKay, E. Galius, I.A. Anderson, The dielectric constant of 3M VHB: a parameter in dispute, in: Proc. SPIE 7287, Electroact. Polym. Actuators Devices, 2009: pp. 72870–72879. http://dx.doi.org/10.1117/12.815821.
[45] J.J. Sheng, H.L. Chen, J.H. Qiang, B. Li, Y.Q. Wang, Thermal, mechanical, and dielectric properties of a dielectric elastomer for actuator applications, J. Macromol. Sci. B 51 (2012) 2093–2104. http://dx.doi.org/10.1080/00222348.2012.659617.
[46] G. Kofod, P. Sommer-Larsen, R. Kornbluh, R. Pelrine, Actuation response of polyacrylate dielectric elastomers, J. Intell. Mater. Syst. Struct. 14 (2003) 787–793. http://dx.doi.org/10.1177/104538903039260.
[47] L. An, F. Wang, S. Cheng, T. Lu, T.J. Wang, Experimental investigation of the electromechanical phase transition in a dielectric elastomer tube, Smart Mater. Struct. 24 (2015) 35006. http://dx.doi.org/10.1088/0964-1726/24/3/035006.
[48] T. Lu, L. An, J. Li, C. Yuan, T.J. Wang, Electro-mechanical coupling bifurcation and bulging propagation in a cylindrical dielectric elastomer tube, J. Mech. Phys. Solids. 85 (2015) 160–175. http://dx.doi.org/10.1016/J.JMPS.2015.09.010.
[49] D. Gatti, H. Haus, M. Matysek, B. Frohnapfel, C. Tropea, H.F. Schlaak, The dielectric breakdown limit of silicone dielectric elastomer actuators, Appl. Phys. Lett. 104 (2014) 2012–2016. http://dx.doi.org/10.1063/1.4863816.